PMIP4/CMIP6 Last Interglacial simulations using different versions of MIROC, with and without vegetation feedback

Ryouta O'ishi[1], Wing-Le Chan[1], Ayako Abe-Ouchi[123], Sam Sherriff-Tadano[1] and Rumi Ohgaito[3]

[1]Atmosphere and Ocean Research Institute, University of Tokyo, Kashiwa, 2778568, Japan
5   [2]National Institute of Polar Research, Tachikawa, 1908518, Japan
[3]Japan Agency for Marine-Earth Science and Technology, Yokohama, 2360001, Japan

Correspondence to: Ryouta O'ishi (ryo@aori.u-tokyo.ac.jp)

Abstract. We carry out a Last Interglacial (LIG) experiment, named lig127k and a Tier1 experiment of PMIP4/CMIP6, using three versions of the MIROC model, MIROC4m, MIROC4m-LPJ and MIROC-ES2L. The results are compared with
10   reconstructions from climate proxy data. All models show summer warming over northern high latitude land, reflecting the differences between the distributions of the LIG and present-day solar irradiance. Only MIROC4m-LPJ, which includes dynamical vegetation feedback from the change in vegetation distribution, shows warming signals, even for the annual mean, at northern high latitudes, as shown by proxy data. However, the latest Earth System Model (ESM) of MIROC, MIROC-ES2L, in which there is only a partial vegetation effect through the leaf area index, shows no change or even annual cooling over
15   large parts of the northern hemisphere. Results from the series of experiments show that the inclusion of vegetation feedback is necessary for the reproduction of the strong annual warming over land at northern high latitudes. The LIG experimental results show that the warming predicted by models is still underestimated, even with dynamical vegetation, compared to reconstructions from proxy data, suggesting that further investigation and improvement to the climate feedback mechanism are needed.

20   **1 Introduction**

The Last Interglacial (LIG, 130ka-116ka) is referred to as the warmest period in the recent glacial-interglacial cycle (NGRIP members 2004, Overpeck et al. 2006). The most important characteristic of the LIG is the strong summer solar irradiance in the northern hemisphere due to the difference in the earth's orbit during that period and that of the present-day (Berger 1978). For example, 127,000 years ago, summer solar irradiance was more than 50W/m^2 larger compared to that of the present-day
25   (Figure 1). Paleo-evidence shows strong warming at northern high latitudes in response to this different spatial and temporal pattern of solar irradiance (Otto-Bliesner et al. 2006, Lund et al. 2013). Northward shift of boreal treeline due to warming is also indicated by proxies (LIGA members 1991, Edwards et al. 2003). Sea level rise due to warming has also been pointed out, with contributions from the mass balance change in the Greenland and the Antarctic ice sheets (Robinson et al. 2011, Born and Nisancioglu, 2012, Quiquet et al. 2013, Stone et al. 2013).

30   The Paleoclimate Modelling Intercomparison Project (PMIP) coordinates the cooperation and comparison between modelling and data of the past (Braconnot et al. 2000, Braconnot et al. 2007, Braconnot et al. 2012). The LIG is one of targeted periods as well as the mid-Holocene and the Last Glacial Maximum (Otto-Bliesner et al. 2017). For the simulation of the past periods, PMIP provides protocols with common settings which should be applied to participating models. In the present study, we apply the LIG boundary conditions provided by the PMIP4 to three different version of atmosphere-ocean coupled general

35   circulation models (AOGCMs) which belong to the Model for Interdisciplinary Research on Climate (MIROC) family and compare results with the pre-industrial simulations, focusing on the different treatment of vegetation among the three models.

2 Models and settings

2.1 Models

2.1.1 MIROC4m

40   An AOGCM, MIROC4m, is based on MIROC3.2 which contributed to the fourth assessment report (AR4; Meehl et al. 2007) of the Intergovernmental Panel on Climate Change (IPCC). MIROC4m consists of Center for Climate System Research Atmosphere General Circulation Model (CCSR AGCM; Hasumi and Emori 2004) and CCSR Ocean Component Model (COCO; Hasumi 2006). The AGCM solves the primitive equations on a sphere using a spectral method (Numaguti et al. 1997). The model resolution of atmosphere component is T42 with vertical 20 layers. The land submodel is the Minimal Advanced

45   Treatments of Surface Interaction and Runoff (MATSIRO; Takata et al. 2003). Vegetation is prescribed to a satellite based present-day distribution. The OGCM solves the primitive equation on a sphere, where the Boussinesq and hydrostatic approximations are adopted (Hasumi 2006). The horizontal resolution is ~1.4° in longitude and 0.56°−1.4° in latitude (latitudinal resolution is finer near the equator). There are 43 vertical layers. It is coupled to a dynamic–thermodynamic sea ice model. These models are used extensively for modern climate (Obase et al. 2017), paleoclimate (Abe-Ouchi et al. 2013;

50   Sherriff-Tadano et al. 2018), and future climate studies (Yamamoto et al. 2015).

2.1.2 MIROC4m-LPJ

We newly developed a vegetation coupled AOGCM MIROC4m-LPJ by introducing the Lund-Potsdam-Jenna Dynamical Global Vegetation Model (LPJ-DGVM; Sitch et al. 2003) into MIROC4m. The coupling method is the same as that used for

55   MIROC-LPJ in previous studies (O'ishi and Abe-Ouchi 2009, 2011, 2013) which adopted a slab ocean instead of full ocean model COCO. In the present study, we apply a direct coupling to avoid bias correction coupling between atmosphere and vegetation components. LPJ-DGVM predicts potential vegetation distribution which is translated to the classification used for MATSIRO annually by using monthly mean temperature, precipitation and cloud cover predicted by the atmosphere component of the GCM. A detailed description of the method can be found in O'ishi and Abe-Ouchi (2009). Another important

60   modification is the introduction of a wetland scheme developed by Nitta et al. (2017). This scheme improves seasonality of the hydrological behaviour over land. When snow melt occurs, a part of melt water does not directly runoff into river but stored

in an isolated storage. This stored water decays with timescale depending on the standard deviation of topography and the decayed amount of water is taken into account of land surface water and energy balance. The introduction of this scheme reduces summer warm bias over land in middle to high latitude. The model resolutions are the same as those of MIROC4m.

65

2.1.3 MIROC-ES2L

An earth system model (ESM) MIROC, Earth System version 2 for long-term simulations (MIROC-ES2L; Hajima et al. 2019/submitted) is one of the contributing models to PMIP4/CMIP6. The physical component of MIROC-ES2L is MIROC5.2 (Tatebe et al. 2018), an upgraded version of MIROC5 (Watanabe et al. 2010) which contributed to the IPCC AR5 (IPCC,

70 2013). The most important update in MIROC-ES2L from previous versions (Watanabe et al. 2011, Kawamiya et al. 2005) is the introduction of a nitrogen cycle. The land nitrogen and carbon cycles are predicted by a modified version of the Vegetation Integrative Simulator for a Trace gas model, VISIT (Ito and Inatomi, 2012a), referred to hereafter as VISIT-e. Vegetation distribution is prescribed in both MATSIRO and VISIT-e, but the leaf area index (LAI) is predicted daily by VISIT-e and transferred to MATSIRO. The ocean nitrogen and carbon cycles are predicted by an ocean biogeochemical component model

75 OECO2. Detailed information is described in Hajima et al. (2019). The model resolution of the atmosphere component is T42 with vertical 40 layers. The model resolution of the ocean component is a warped tripolar coordinate system with longitudinal 1° grid spacing in the spherical coordinate portion south of 63°N and meridional grid spacing varying from 0.5° (near equator) to 1° (mid-latitudes). The number of vertical layers is set to 63.

2.2 Settings

80 In the present study, three models are run with the same forcings and with the boundary conditions of the pre-industrial (*piControl* in PMIP4/CMIP6, hereafter PI) and of the Last Interglacial (*lig127k* in PMIP4, hereafter 127k), as shown in Table 1, following the PMIP4/CMIP6 protocol (Otto-Bliesner et al. 2017). The orbital forcings in both experiments are as same as those recommended in Otto-Bliesner et al. 2017. The greenhouse gas (GHG) concentrations in piControl are slightly different from Otto-Bliesner et al. (2017). We apply GHG values from the CMIP3 control experiment using MIROC3.2 to MIROC4m

85 and MIROC4m-LPJ and those from the CMIP6 DECK *piControl* experiment using MIROC-ES2L (Hajima et al. 2019) to MIROC-ES2L. Details of these GHG values are shown in Table 1. The GHG concentrations in the 127k experiments are the same as those specified in Otto-Bliesner et al. (2017). Paleogeography and ice sheet are set to modern in all experiments. Vegetation distribution in MIROC4m is fixed to a present-day vegetation according to Ramankutty and Foley (1999); see Figure 3. In MIROC4m-LPJ, vegetation distribution is predicted as same as MIROC-LPJ (O'ishi and Abe-Ouchi 2006). In

90 MIROC-ES2L, vegetation distribution is fixed to a satellite based vegetation distribution (Matthews 1983, Matthews 1984, Hall et al. 2006) as the same as that in MATSIRO of MIROC5 (Watanabe et al. 2010) (see Figure 2) and as the same as that in the DECK *piControl* experiment (Hajima et al. 2019) using VISIT-e. However, as described above, VISIT-e predicts the leaf area index (LAI) which is referred by MATSIRO. In all experiments, the last 100 years, during which the climate has reached equilibrium, are used for analysis.

3 Results

3.1 Temperature

Seasonally and annually averaged surface air temperature difference between the 127k from PI are shown in Figure 4. All models show the largest warming (>6K) in June-July-August (JJA) and global cooling in December-January-February (DJF) which corresponds to increased boreal summer solar irradiance and decreased boreal winter solar irradiance in the LIG, respectively. In September-October-November (SON), there is a switch to cooling over northern hemisphere land at middle and high latitudes. On the other hand, warming (>3K) occurs across Antarctica in all models, reflecting the increase of solar irradiance at SH high latitudes in SON. In March-April-May (MAM), the global cooling is less than that in DJF and warming is seen at northern high latitudes.

The change in annually averaged surface air temperature is smaller than that of the seasonally averaged value because summer warming is compensated by cooling in other seasons. MIROC4m shows global cooling except for some isolated areas where annual temperatures are higher, eg Greenland. MIROC4m-LPJ show annual warming (at most 3K) in both high latitude land and in the Arctic Ocean with vegetation change from tundra to boreal forest in northern coast of Eurasia and North America (Figure 3). Especially in MAM, only MIROC4m-LPJ shows strong warming in Alaska and Eastern Siberia. The Arctic Ocean show warming throughout all seasons in MIROC4m-LPJ, which is not seen in MIROC4m and MIROC-ES2L. MIROC-ES2L, as well as MIROC4m-LPJ, show annual warming in the Arctic Ocean, but the intensity in the former model is less. MIROC-ES2L shows annual warming in Antarctica which is not seen in the other two models.

May-June-July-August (MJJA) averaged temperature difference is shown in Figure5, focusing on Greenland. MIROC4m and MIROC4m-LPJ show similar pattern of warming which is larger as the altitude is higher. MIROC-ES2L shows more homogeneous warming pattern over Greenland and intensity of warming is weaker than former two models.

Simulated temperature changes are compared with reconstructed values from proxies. In Figure 6, annual surface temperature change is compared with land proxies by Turney and Jones (2010), hereafter referred to as TJ2010. MIROC4m-LPJ exhibits the largest warming among three models at northern high latitudes. However, the agreement with TJ2010 is not quantitative but just qualitative; annual warming is still underestimated. The other two models show cooling in northern high latitude land. Greenland warming appears in all models, but is smaller than that of TJ2010. In Antarctica, MIROC-ES2L shows the same sign of temperature change as in TJ2010, but the intensity (at most +1K) is weaker than that of TJ2010. MIROC4m and MIROC4m-LPJ show cooling rather than warming in Antarctica. In Figure 7, annual surface temperature change is compared with a newer reconstruction by Capron et al. (2017), hereafter referred to as C2017. All models show warming in Greenland, but only MIROC-ES2L reproduces Antarctica warming. The models underestimate warming at all sites in C2017 as the intensity is not reproduced.

Figure 8 compares the simulated annual sea surface temperature (SST) change and TJ2010 ocean proxies. All three models predict warm SST at northern high latitudes and cooling at low latitudes. This large-scale latitudinal pattern agrees with TJ2010, but some individual sites disagree in terms of sign. For example, the NH SST warming is more substantial in MIROC4m-LPJ

and in MIROC-ES2L than in MIROC4m. The largest warming in the SH is seen in MIROC-ES2L. However, the intensity of SST changes in all models is far smaller than that of TJ2010. We also compare model annual SST difference with newer reconstructions by C2017 and Hoffman et al (2017), hereafter referred to as H2017, in Figure 9. MIROC4m underestimates warming in the northern Atlantic Ocean and shows changes of opposite sign in the southern part of the Pacific and Indian Oceans. MIROC4m-LPJ shows larger warming in NH than in MIROC4m. However, as with MIROC4m, warming in SH is not simulated. MIROC-ES2L predicts better warming in the northern Atlantic Ocean than those of MIROC4m/MIROC4m-LPJ. MIROC-ES2L also predicts improved warming in SH which are partially consistent with proxies. Summer temperature change in the models are compared with that of reconstructions by C2017 and H2017 in Figure 10. Across the wide expanse of the northern Atlantic Ocean, all models predict warming whose sign is consistent with that of reconstructions, except for some cooling sites. MIROC4m-LPJ predicts the largest warming (at most > +4K) while the other two models show a smaller intensity of warming (at most +3K) in the northern Atlantic Ocean. On the other hand, in SH, MIROC4m and MIROC4m-LPJ show cooling in contrast to the warming indicated by proxies. MIROC-ES2L show warming across much of the Southern Ocean, in contrast to the other two models. However, some sites still indicate an opposite sign to that of proxies.

3.2 Precipitation, sea ice and vegetation

3.2.1 Precipitation

The precipitation change between 127k and PI is indicated in Figure 11. In general, similar annually averaged precipitation changes are seen in all three models. Precipitation increase occurs in subtropical arid areas in the northern hemisphere, especially in Africa. MIROC4m and MIROC4m-LPJ show almost the same precipitation change since they share the same atmosphere component. MIROC-ES2L shows a pattern slightly different to that of the MIROC4m models.

Figure 12 shows JJA zonally averaged precipitation over Sahara (30W-20E). In all models, 127k summer precipitation shifts northward compared to PI. MIROC4m-LPJ shows the largest northward shift of precipitation. MIROC4m predicts slight northward expansion of vegetation compared with that of PI reflecting the precipitation increase. However, vegetation distribution in Sahara does not show a significant northward expansion known as the "green Sahara".

3.2.2 Sea ice

In figure 13, March NH sea ice thickness in PI, 127k and their difference (127k-PI) are shown for all three models. The PI sea ice distribution show characteristics common in both MIROC4m and MIROC4m-LPJ. The highest values appear from the North Pole to eastern Siberia. MIROC-ES2L shows a pattern different to the two MIROC4m models. The highest values appear from the North Pole to North America. This is due to the different ocean and sea ice model adopted in the physical part of MIROC-ES2L. This different characteristic is also seen in 127k. The resultant difference between 127ka and PI sea ice distribution also differs between the MIROC4m-based models and MIROC-ES2L. The largest reduction in sea ice occurs along the eastern Siberian coast in the MIROC4m-based models, although MIROC-ES2L shows the largest reduction on the eastern coast of Greenland. MIROC4m and MIROC4m-LPJ show differences in spite of their common ocean and sea ice

models. The sea ice thickness is smaller in MIROC4m-LPJ than in MIROC4m although they show a similar distribution pattern. This is due to different equilibrium temperatures in MIROC4m and MIROC4m-LPJ. The PI equilibrium temperature in MIROC4m-LPJ is slightly higher (not shown) than that of MIROC4m due to the inclusion of a vegetation component. Figure

165   14 shows September NH sea ice thickness. As well as in March, MIROC-ES2L shows a different distribution of sea ice and response in 127k compared to MIROC4m-based models. MIROC4m-LPJ shows the smallest sea ice thickness among the three models in both PI and 127k which corresponds to a warm Arctic Ocean in both PI and 127k. MIROC4m-LPJ predicts obviously less sea ice in September in PI compared to observation (e.g. HadISST; Rayner et al. 2003). March SH sea ice thickness is shown in Figure 15. In the Southern Ocean, all models show sea ice thickness to be thinner than that in the Arctic Ocean.

170   March sea ice shows the same characteristics in the two MIROC4m-based models. MIROC-ES2L shows a different pattern, and the smallest amount of sea ice, compared with MIROC4m-based models. In all three models, March sea ice increases in 127k but the intensity differs depending on the model as well as NH. September SH sea ice thickness is shown in Figure 16. As in March, there is a discrepancy between the sea ice thickness distributions of the MIROC4m-based models and MIROC-ES2L. Sea ice in the PI is smaller in MIROC-ES2L and the response of sea ice in 127k is also the smallest in that model.

175   MIROC-ES2L clearly underestimates sea ice in both season compared to observation.

3.2.3 Vegetation

We compare the vegetation distribution in all three models (Figure 3) regardless of different treatment (prescribed or predicted). MIROC4m and MIROCES2L adopt a fixed vegetation distribution based on satellite data. Vegetation distribution in

180   MIROC4m is based on the classification of MATSIRO, translated from actual vegetation by Ramankutty and Foley (1999). MIROC-ES2L is also fixed to satellite-based vegetation distribution which is translated from satellite data (Matthews 1983, Matthews 1984, Hall et al. 2006). These two vegetation maps show similar patterns of forest and grassland, although differ in the interpretation of classification such as C3/C4 or the boundary between forest and tundra. Only MIROC4m-LPJ predicts vegetation distribution in the present study. The 100-year averaged vegetation distribution in the PI shows characteristics

185   common with the other two satellite-based distributions, except for the overestimation of forests (in boreal forest band and African tropical forest) and underestimation of grassland (in African Savanna and central Eurasia). In the 127k simulation, vegetation drastically changes at northern high latitudes. Tundra is broadly replaced by boreal deciduous forest and almost disappears, reflecting the summer warming in the northern high-latitude land especially in Eastern Siberia and North America. Forestation of tundra regions causes amplification of warming at Eastern Siberia and North America, especially in the snow

190   melting season. This northward shift of boreal forest finally affects by +3K annually averaged temperature in Eastern Siberia and North America compared with LIG warming without vegetation change. Grassland appears at the wide area of boreal-temperate boundary in both Eurasia and North America due to less precipitation to support forests in 127k. This increase of grassland causes cooling at middle latitudes, especially in Eurasia. In Sahara, slight northward expansion of grassland is seen, but MIROC4m-LPJ did not reproduce so called "green Sahara".

4 Conclusions and Discussions

In the present study, we examined the LIG and PI simulations in accordance to the PMIP4 protocol by using three different versions of the MIROC AOGCM. These three models show basically the same response of temperature to the LIG boundary conditions, ie warming in boreal summer and cooling in boreal winter (Figure 4). However, the annually averaged temperature is different among the models. Only MIROC4m-LPJ predicts annual warming at NH high latitudes qualitatively consistent with proxy data such as TJ2010, C2017 and H2017, while the other two models show a cooling at NH high latitudes.

The vegetation change seen in MIROC4m-LPJ simulations is a reasonable response to temperature change induced by orbital parameter. The largest change is the northward shift of boreal forest and expansion of grassland in middle latitude. By comparing MIROC4m-LPJ and MIROC4m, we suggest that the vegetation feedback mechanism is necessary to explain the temperature change reconstructed by proxies since MIROC4m-LPJ predicts closer warming to reconstructions. By considering the overestimation of forest in PI, vegetation feedback may be still underestimated in MIROC4m-LPJ. The introduction of dynamical vegetation in MIROC4m-LPJ appears to amplify the warming not only over land but also in the ocean at NH high latitudes. On the other hand, MIROC-ES2L, which partially introduces a vegetation effect through LAI prediction, does not show enough warming in LIG, but even shows annual cooling over land in the northern high latitude. This result indicates that vegetation feedback including change of vegetation distribution is necessary to predict warm climate both in past and in future. Moreover, it is also pointed out that even MIROC4m-LPJ underestimate warming in spite of the large climate sensitivity (about 4 deg C) of AGCM of MIROC4m among GCMs (Meehl et al. 2007).

Compared to observation, MIROC-ES2L shows most realistic PI distribution of sea ice in the Arctic Ocean, owing to a new ice physics model. MIROC4m-LPJ predicts the smallest amount of sea ice in PI among three models in both March and September, because temperature in MIROC4m-LPJ is generally higher than that of MIROC4m over land due to the inclusion of dynamical vegetation. This warm bias reduces sea ice in the Arctic Ocean in the pre-industrial and thus inevitably affects on the warming in LIG. To investigate the mechanisms in detail, we are planning further feedback analysis focusing on surface energy balance.

5 Code and Data availability

The code of MIROC-ES2L, MIROC4m, MIROC4m-LPJ are not publicly archived because of the copyright policy of MIROC community. Readers are requested to contact the corresponding author if they wish to validate the model configurations of MIROC family models and conduct replication experiments. The source codes, required input data, and simulation results will be provided by the modeling community to which the author belongs. The output of the piControl and lig127k from MIROC-ES2L will be distributed and made freely available through the Earth System Grid Federation (ESGF). Details on the ESGF can be found on the website of the CMIP Panel (https://www.wcrp-climate.org/wgcm-cmip/wgcm-cmip6). All experiments done by MIROC4m and MIROC4m-LPJ will be available from following FTP server (ftp://157.82.240.174/~ryo/cp-2019-172/).

6 Author contribution

230 All authors contributed to the writing of the paper. RO[1] wrote the draft and carried out the analysis. The model simulations were carried out by RO[1] and WLC. RO[3] made arrangements and supported the simulation. RO[1], WLC, RO[3], SST and AAO participated in discussion. AAO coordinated the study.

7 Competing interests

235 The authors declare no competing interests.

Acknowledgement

This work was partially carried out in the Arctic Challenge for Sustainability (ArCS) Project.

240 References

Abe-Ouchi, A., Saito, F., Kawamura, K., Raymo, M. E., Okuno, J., Takahashi, K., and Blatter, H.: Insolation-driven 100,000-year glacial cycles and hysteresis of ice-sheet volume, Nature, 500, 190–193, doi:10.1038/nature12374, 2013.

Berger, A. L. , Long term variations of daily insolation and quaternary climatic changes, J. Atmos. Sci., 13, 2362–2367, 245 https://doi.org/10.1175/1520-0469(1978)035<2362:LTVODI>2.0.CO;2, 1978.

Born, A. and Nisancioglu, K. H.: Melting of Northern Greenland during the last interglaciation, The Cryosphere, 6, 1239–1250,doi:10.5194/tc-6-1239-2012, 2012.

250 Braconnot, P., S. Joussaume, N. de Noblet, and G. Ramstein, Mid-Holocene and last glacial maximum African monsoon changes as simulated within the Paleoclimate Modeling Intercomparison project, Global and Planetary Change, 26, 51-66, doi:10.1016/S0921-8181(00)00033-3, 2000

Braconnot, P., Otto-Bliesner, B., Harrison, S., Joussaume, S., Peterchmitt, J.-Y., Abe-Ouchi, A., Crucifix, M., Driesschaert, 255 E., Fichefet, Th., Hewitt, C. D., Kageyama, M., Kitoh, A., Laîné, A., Loutre, M.-F., Marti, O., Merkel, U., Ramstein, G., Valdes, P., Weber, S. L., Yu, Y., and Zhao, Y.: Results of PMIP2 coupled simulations of the Mid-Holocene and Last Glacial Maximum – Part 1: experiments and large-scale features, Clim. Past, 3, 261–277, https://doi.org/10.5194/cp-3-261-2007, 2007

Braconnot, P., Harrison, S., Kageyama, M. et al. Evaluation of climate models using palaeoclimatic data. Nature Clim. Change

260   2, 417–424, doi:10.1038/nclimate1456, 2012.

Capron, E., Govin, A., Feng, R., Otto-Bliesner, B., and Wolff,E.: Critical evaluation of climate syntheses to benchmarkCMIP6/PMIP4 127 ka Last Interglacial simulations in thehigh-latitude regions, Quaternary Sci. Revi., 168, 137–150,https://doi.org/10.1016/j.quascirev.2017.04.019, 2017.

265

Edwards, M. E., Hamilton, T. D., Elias, S. A., Bigelow, N. H., and Krumhardt, A. P.: Interglacial extension of the boreal forest limit in the Noatak Valley, northwest Alaska: Evidence from an exhumed river-cut bluff and debris apron, Arct. Antarct. Alp. Res., 35, 460–468, 2003.

270   Hajima, T., Watanabe, M., Yamamoto, A., Tatebe, H., Noguchi, M. A., Abe, M., Ohgaito, R., Ito, A., Yamazaki, D., Okajima, H., Ito, A., Takata, K., Ogochi, K., Watanabe, S., and Kawamiya, M.: Description of the MIROC-ES2L Earth system model and evaluation of its climate–biogeochemical processes and feedbacks, Geosci. Model Dev. Discuss., https://doi.org/10.5194/gmd-2019-275, in review, 2019.

275   Hall, D. K., Riggs, G. A. and Salomonson, V. V.: MODIS/Terra Snow Cover 5-Min L2 Swath 500m. Version 5. Boulder, Colorado USA: NASA National Snow and Ice Data Center Distributed Active Archive Center. http://dx.doi.org/10.5067/ACYTYZB9BEOS, 2006.

Hasumi, H.: CCSR Ocean Component Model (COCO), version 4.0, center for Climate System Research Report 25,

280   103 pp., available at: http://www.ccsr.u-tokyo.ac.jp/~hasumi/COCO/coco4.pdf, 2006.

Hasumi, H. and Emori, S.: K-1 Coupled GCM (MIROC) Description, k-1 Technical Report No. 1, Center for Climate System Research (CCSR, Univ. of Tokyo), National Institute for Environmental Studies (NIES), Frontier Research Center for Global Change (FRCGC), 2004.

285

Hoffman, J. S., Clark, P. U., Parnell, A. C., and He, F.: Regional and global sea-surface temperatures during the last interglaciation, Science, 355, 276–279, https://doi.org/10.1126/science.aai8464,2017.

IPCC, 2013: Climate Change: The Physical Science Basis, Contri-bution of Working Group I to the Fifth Assessment Report

290   of theIntergovernmental Panel on Climate Change, edited by: Stocker,T. F., Qin, D., Plattner, G.-K., Tignor, M., Allen, S. K., Boschung,J., Nauels, A., Xia, Y., Bex, V., and Midgley, P. M., CambridgeUniversity Press, Cambridge, United Kingdom and New York,NY, USA, 1535 pp., doi:10.1017/CBO9781107415324, 2013

Ito, A. and Inatomi, M.: Water-use efficiency of the terrestrial biosphere: A model analysis focusing on interactions between

295   the global carbon and water cycles, J. Hydrometeorol., 13(2), 681–694, doi:10.1175/JHM-D-10-05034.1, 2012

Kawamiya, M., Yoshikawa, C., Kato, T., Sato, H., Sudo, K., Watan-abe, S., and Matsuno, T.: Development of an Integrated
EarthSystem Model on the Earth Simulator, J. Earth Sim., 4, 18–30,2005

300   LIGA members: The last interglacial in high latitudes of the North-ern Hemisphere: Terrestrial and marine evidence, Quatern.
Int., 10–12, 9–28, doi:10.1016/1040-6182(91)90038-P, 1991.

Lunt, D. J., Abe-Ouchi, A., Bakker, P., Berger, A., Braconnot, P., Charbit, S., Fischer, N., Herold, N., Jungclaus, J. H., Khon,
V. C., Krebs-Kanzow, U., Langebroek, P. M., Lohmann, G., Nisancioglu, K. H., Otto-Bliesner, B. L., Park, W., Pfeiffer, M.,
305   Phipps, S. J., Prange, M., Rachmayani, R., Renssen, H., Rosenbloom, N., Schneider, B., Stone, E. J., Takahashi, K., Wei, W.,
Yin, Q., and Zhang, Z. S.: A multi-model assessment of last interglacial temperatures, Clim. Past, 9, 699–717,
https://doi.org/10.5194/cp-9-699-2013, 2013

 Matthews, E.: Global vegetation and land cover: New high-resolution data bases for climate studies. J. Clim. Appl. Meteor.
310   22, 474-487, 1983.

Matthews, E.: Prescription of Land-surface Boundary Conditions in GISS GCM II: A Simple Method Based on High-
resolution Vegetation Data Sets. NASA TM-86096. National Aeronautics and Space Administration. Washington, D.C., 1984.

315   Meehl, G. A., Stocker, T. F., Collins, W. D., Friedlingstein, P., Gaye,A. T., Gregory, J. M., Kitoh, A., Knutti, R., Murphy, J.
M., Noda,A., Raper, S. C. B., Watterson, I. G., Weaver, A. J., and Zhao,Z.-C.: Global Climate Projections, in: Climate
Change 2007:The Physical Science Basis. Contribution of Working Group Ito the Fourth Assessment Report of the
Intergovernmental Panelon Climate Change, edited by: Solomon, S., Qin, D., Manning,M., Chen, Z., Marquis, M., Averyt, K.
B., Tignor, M., and Miller,H. L., Cambridge University Press, Cambridge, United Kingdomand New York, NY, USA, 2007.
320
NGRIP members: High-resolution record of Northern Hemisphereclimate extending into the last interglacial period, Nature,
431,147–151,doi:10.1038/nature02805, 2004

Nitta, T., Yoshimura, K., and Abe-Ouchi, A.: Impact of arctic wetlands on the climate system: Model sensitivity simulations
325   with the MIROC5 AGCM and a snow-fed wetland scheme, J. Hydrometeorol., 18, 2923–2936, https://doi.org/10.1175/JHM-
D-16-0105.1, 2017.

Numaguti, A., M. Takahashi, T. Nakajima, A. Sumi: Description of CCSR/NIES atmospheric general circulation model CGER's Supercomputer Monograph Report, 3, Center for Global Environmental Research, National Institute for 330 Environmental Studies (1997)

Obase, T., Abe-Ouchi, A., Kusahara, K., Hasumi, H., and Ohgaito, R.: Responses of basal melting of Antarctic ice shelves to the climatic forcing of the Last Glacial Maximum and CO2 doubling, J. Climate, 30, 3473–3497, https://doi.org/10.1175/JCLI-D-15-0908.1 , 2017.

335

O'ishi, R. and Abe-Ouchi, A.: Influence of dynamic vegetation on climate change arising from increasing CO2, Clim. Dynam., 33, 645–663, https://doi.org/10.1007/s00382-009-0611-y, 2009.

O'ishi, R. and Abe-Ouchi, A.: Polar amplification in the mid-Holocene derived from dynamical vegetation 340 change with a GCM, Geophys. Res. Lett., 38, L14702, doi:10.1029/2011GL048001, 2011.

O'ishi, R. and Abe-Ouchi, A.: Influence of dynamic vegetation on climate change and terrestrial carbon storage in the Last Glacial Maximum, Clim. Past, 9, 1571–1587, https://doi.org/10.5194/cp-9-1571-2013, 2013.

345 Otto-Bliesner, B., Marshall, S. J., Overpeck, J. T., Miller, G. H., Hu, A., and CAPE Last Inter-glacial Project Members: Simulating Arctic climate warmth and icefield retreat in the lastinterglaciation, Science, 311, 1751–1753, doi: 10.1126/science.1120808, 2006.

Otto-Bliesner, B. L., Braconnot, P., Harrison, S. P., Lunt, D. J., Abe-Ouchi, A., Albani, S., Bartlein, P. J., Capron, E., Carlson, 350 A. E., Dutton, A., Fischer, H., Goelzer, H., Govin, A., Haywood, A., Joos, F., LeGrande, A. N., Lipscomb, W. H., Lohmann, G., Mahowald, N., Nehrbass-Ahles, C., Pausata, F. S. R., Peterschmitt, J.-Y., Phipps, S. J., Renssen, H., and Zhang, Q.: The Pfeiffer, M. and Lohmann, G.: Greenland Ice Sheet influence on Last Interglacial climate: global sensitivity studies performed with an atmosphere–ocean general circulation model, Clim. Past, 12, 1313–1338, https://doi.org/10.5194/cp-12-1313-2016, 2016.

355

Overpeck, J. T., Otto-Bliesner, B., Miller, G. H., Muhs, D. R., Alley, R. B., and Kiehl, J. T.: Paleoclimatic evidence for future ice-sheet instability and rapid sea-level rise, Science, 311,1747–1750,doi:10.1126/science.1115159, 2006.

PMIP4 contribution to CMIP6 – Part 2: Two interglacials, scientific objective and experimental design for Holocene and Last 360 Interglacial simulations, Geosci. Model Dev., 10, 3979–4003, https://doi.org/10.5194/gmd-10-3979-2017, 2017.

Quiquet, A., Ritz, C., Punge, H. J., and Salas y M´elia, D.: Greenland ice sheet contribution tosea level rise during the last interglacial period: a modelling study driven and constrained byice core data, Clim. Past, 9, 353–366,doi:10.5194/cp-9-353-2013, 2013

365

Ramankutty, N. and Foley, J. A.: Estimating historical changes in global land cover: Croplands from 1700 to 1992, Glob. Biogeochem. Cy., 13, 997–1027, https://doi.org/10.1029/1999GB900046, 1999.

Rayner, N. A., D. E. Parker, E. B. Horton, C. K. Folland, L. V. Alexander, D. P. Rowell, E. C. Kent, and A. Kaplan, Global

370 analyses of sea surface temperature, sea ice, and night marine air temperature since the late nineteenth century, J. Geophys. Res., 108(D14), 4407–37, doi:10.1029/2002JD002670, 2003.

Robinson, A., Calov, R., and Ganopolski, A.: Greenland ice sheet model parameters con-strained using simulations of the Eemian Interglacial, Clim. Past, 7, 381–396,doi:10.5194/cp-7-381-2011, 2011

375

Sherriff-Tadano, S., Abe-Ouchi, A., Yoshimori, M., Oka, A., andChan, W.-L.: Influence of glacial ice sheets on the Atlanticmeridional overturning circulation through surface wind change, Clim. Dynam., 50, 2881–2903, https://doi.org/10.1007/s00382-017-3780-0, 2018.

380 Sitch, S., Smith, B., Prentice, I. C., Arneth, A., Bondeau, A., Cramer, W., Kaplan, J. O., Levis, S., Lucht, W., Sykes, M. T., Thonicke, K., and Venevsky, S.: Evaluation of ecosystem dynamics, plant geography and terrestrial carbon cycling in the LPJ dynamic global vegetation model, Glob. Change Biol., 9, 161–185, doi:10.1046/j.1365-2486.2003.00569.x, 2003.
Stone, E. J., Lunt, D. J., Annan, J. D., and Hargreaves, J. C.: Quantification of the Greenland ice sheet contribution to Last Interglacial sea level rise, Clim. Past, 9, 621–639, https://doi.org/10.5194/cp-9-621-2013, 2013.

385

Takata, K., Emori, S., and Watanabe, T.: Development of the minimal advanced treatments of surface interaction and runoff, Global Planet. Change, 38, 209–222, 2003.

Tatebe, H., Tanaka, Y., Komuro, Y. et al. Impact of deep ocean mixing on the climatic mean state in the Southern Ocean. Sci

390 Rep 8, 14479, doi:10.1038/s41598-018-32768-6, 2018

Turney, C. S. M. and Jones, R. T.: Does the Agulhas Current amplifyglobal temperatures during super-interglacials?, J. Quat. Sci., 25,839–843, 2010.

395   Watanabe, M., Suzuki, T., O'ishi, R., Komuro, Y., Watanabe, S., Emori, S., Takemura, T., Chikira, M., Ogura, T., 2040Sekiguchi, M., Takata, K., Yamazaki, D., Yokohata, T., Nozawa, T., Hasumi, H., Tatebe, H. and Kimoto, M.: Improved climate simulation by MIROC5: Mean states, variability, and climate sensitivity, J. Clim., 23(23), 6312–6335, doi:10.1175/2010JCLI3679.1, 2010

400   Watanabe,S., Hajima, T., Sudo, K., Nagashima, T., Takemura, T., Okajima, H., Nozawa, T., Kawase, H., Abe, M., Yokohata, T., Ise, T., Sato, H., Kato, E., Takata, K., Emori, S. and Kawamiya, M.: MIROC-ESM 2010: Model description 2045and basic results of CMIP5-20c3m experiments, Geosci. Model Dev., 4(4), 845–872, doi:10.5194/gmd-4-845-2011, 2011.

       Yamamoto, A., Abe-Ouchi, A., Shigemitsu, M., Oka, A., Takahashi,K., Ohgaito, R., and Yamanaka, Y.: Global deep
405   ocean oxy-genation by enhanced ventilation in the Southern Ocean underlongterm global warming, Global Biogeochem. Cy., 29, 1801–1815, 2015.

	piControl	*lig127k*
Eccentricity	0.01672	0.039378
Obliquity (degrees)	23.45	24.04
Perihelion – 180 (degrees)	102.04	275.41
Carbon dioxide (ppm)	285.431 / 284.725	275
Methane (ppb)	863.303 / 808.249	685
Nitrous oxide (ppb)	279.266 / 273.021	255
Solar constant (W/m^2)	1366.12	Same as in *piControl*
Paleogeography	Modern	Same as in *piControl*
Ice sheets	Modern	Same as in *piControl*
Vegetation	Prescribed or interactive	Prescribed as in *piControl* or interactive (depends on model)

410   Table 1: Forcings and boundary conditions of Pre-Industrial (*piControl*) and the Last Interglacial (*lig127k*). Greenhouse gases with MIROC-ES2L are shown after / in the *piControl*.

Experiment	Model name	Model type	Vegetation	Int. length
piControl	MIROC4m	AOGCM	Prescribed	4000 yrs

piControl	MIROC4m-LPJ	AOVGCM	Interactive	2000 yrs
piControl	MIROC-ES2L	ESM	Prescribed	500 yrs
lig127k	MIROC4m	AOGCM	Prescribed	3000 yrs
lig127k	MIROC4m-LPJ	AOVGCM	Interactive	3000 yrs
lig127k	MIROC-ES2L	ESM	Prescribed	1550 yrs

415   Table 2: List of experiments
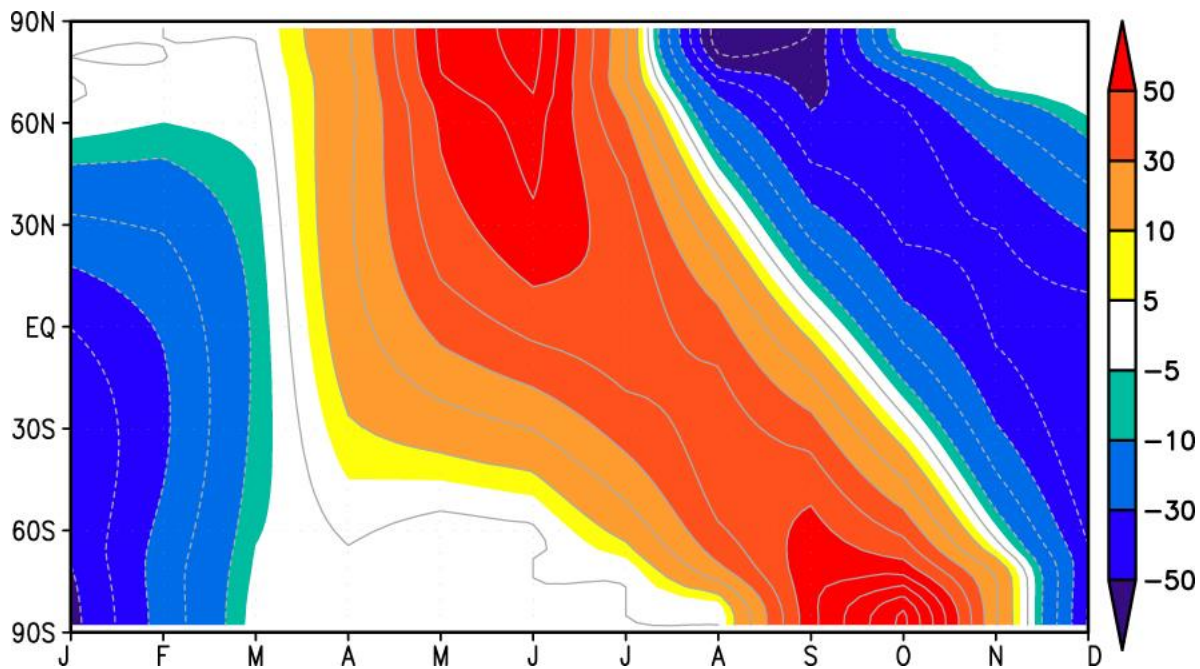
Figure 1: Latitude-month insolation anomaly between 127ka and present-day (W/m²). Modern calendar is assumed.

420

425
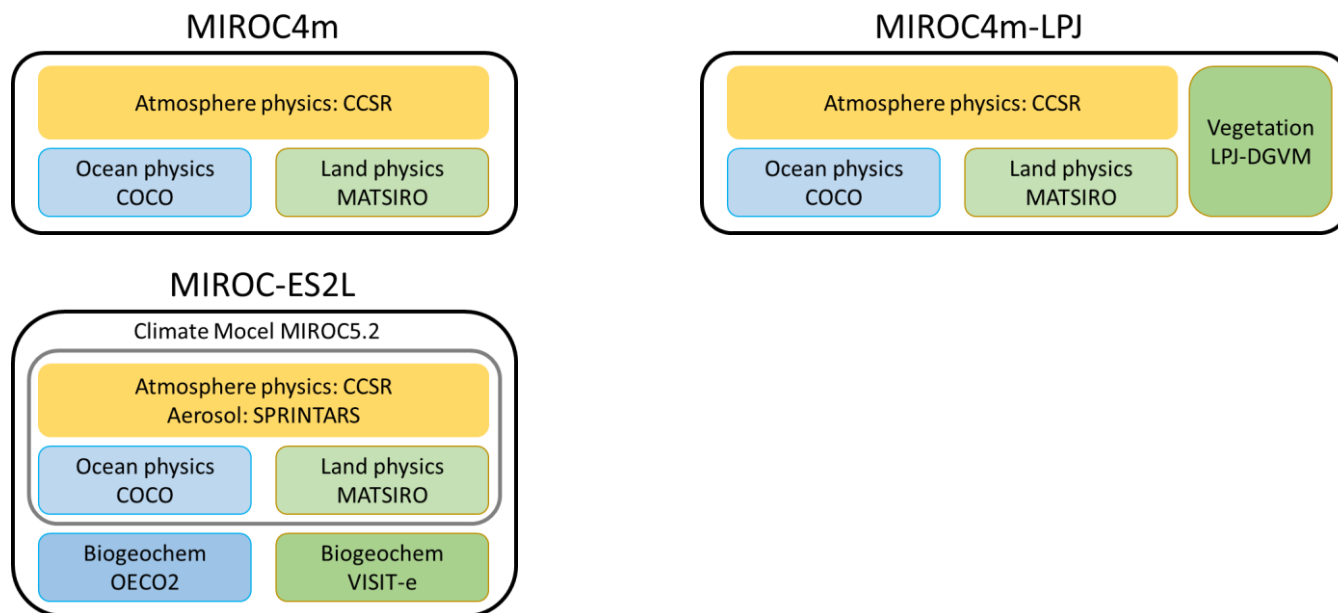
430   Figure 2: schematic of models
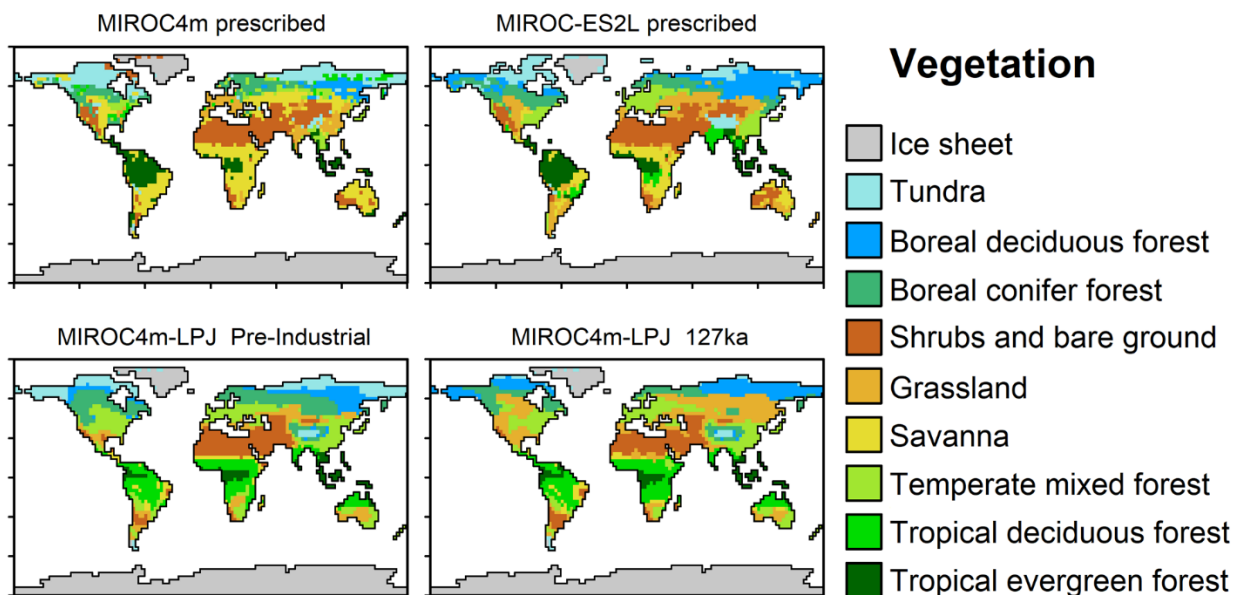
Figure 3: Vegetation distribution as fixed boundary condition (MIROC4m and MIROC-ES2L) and resultant most dominant
vegetation types in MIROC4m-LPJ experiments in PI and 127k.
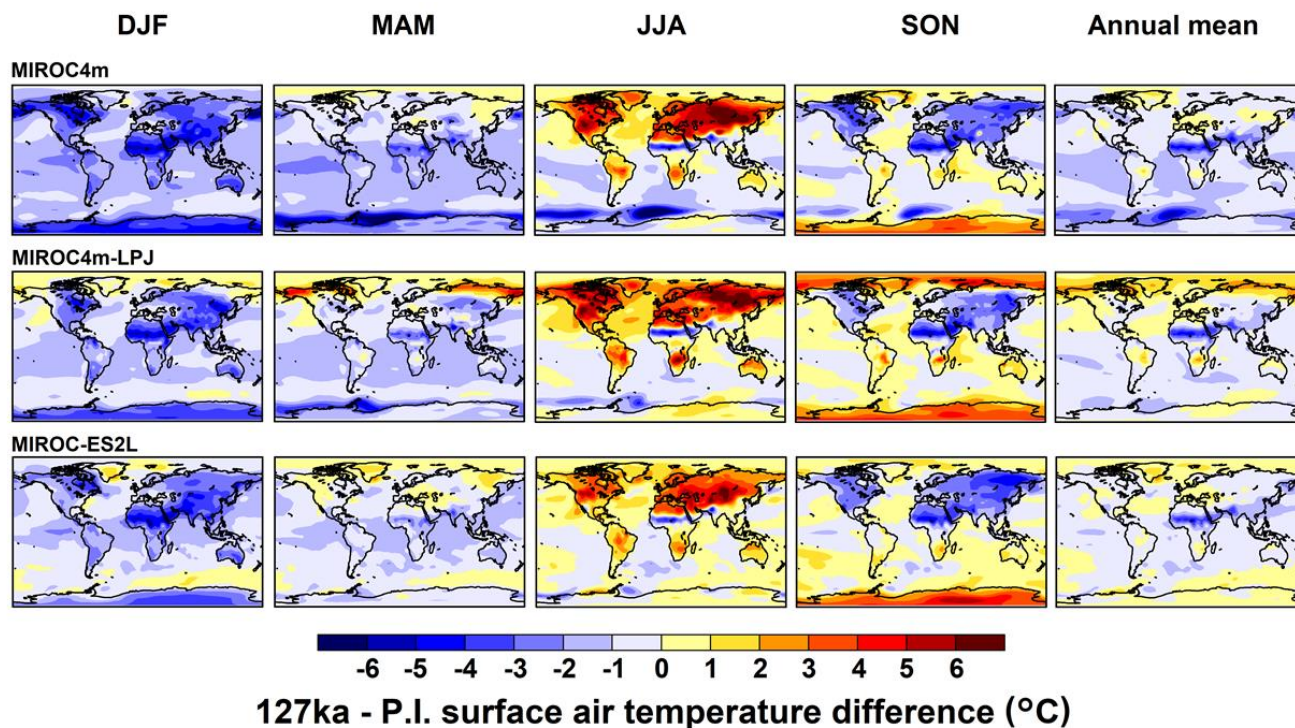
Figure 4: Seasonal and annual surface air temperature difference (ºC) between 127k and PI in three models. The present-day
calendar is applied to both PI and 127k.
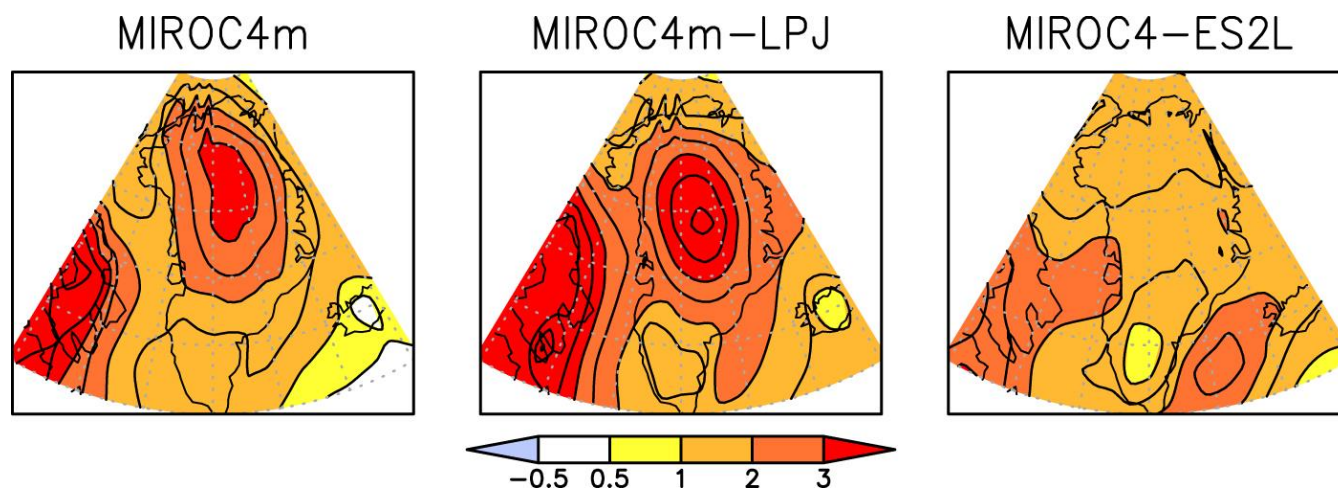
Figure 5: May-June-July-August averaged temperature difference (K) between 127k and PI in three models. The present-day calendar is applied to both PI and 127k.
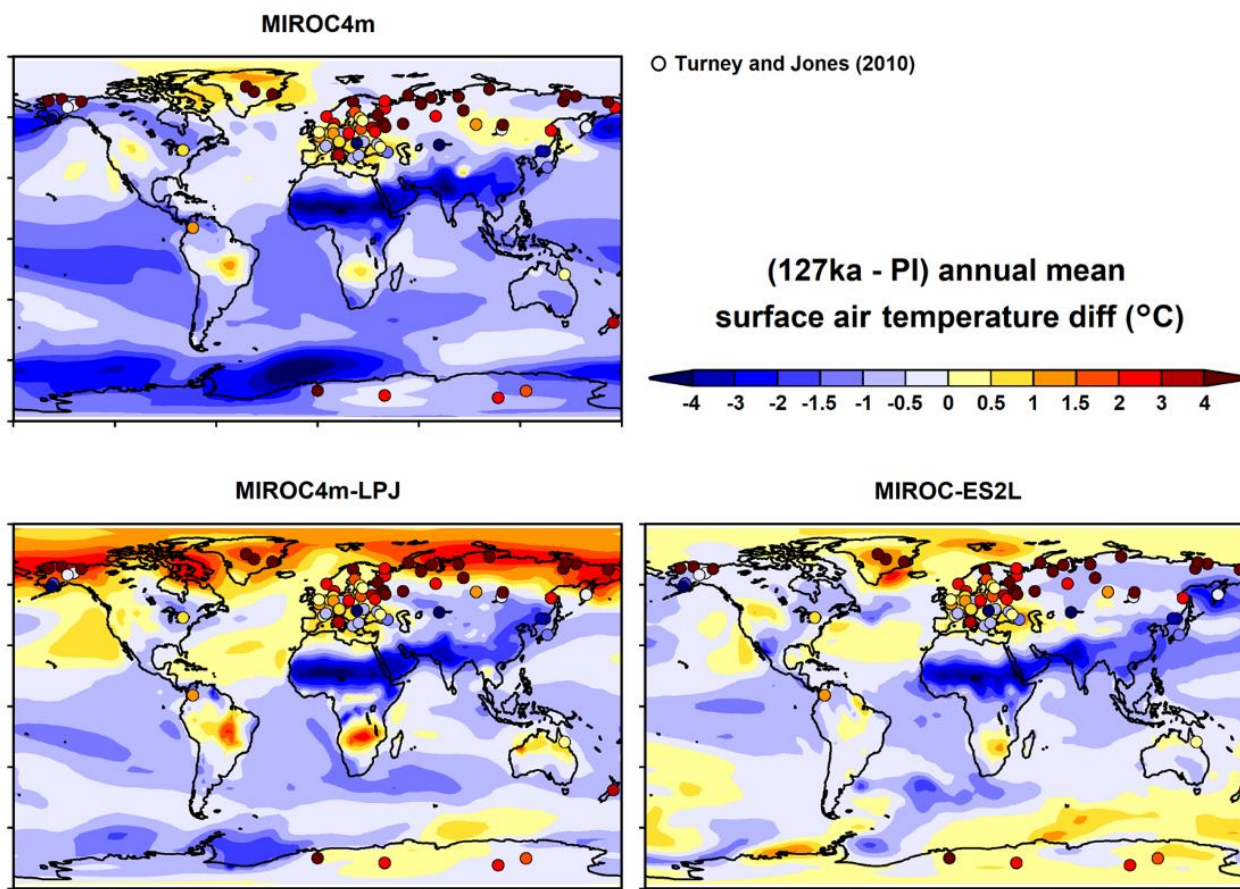
445

Figure 6: Annual surface air temperature change between 127k and PI is compared with reconstruction by Turney and Jones (2010)
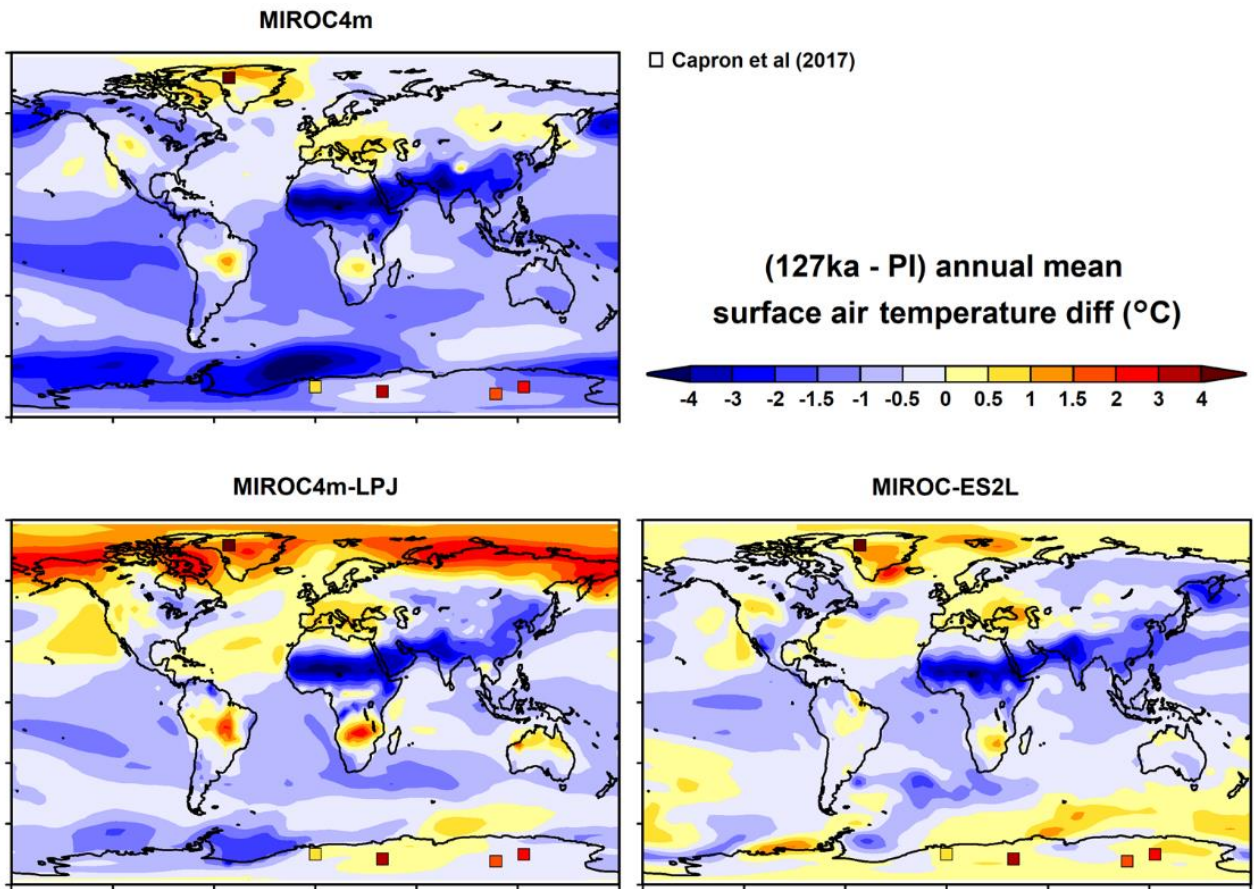
Figure 7: As same as Figure 6 but compared with reconstruction by Capron et al. (2017).
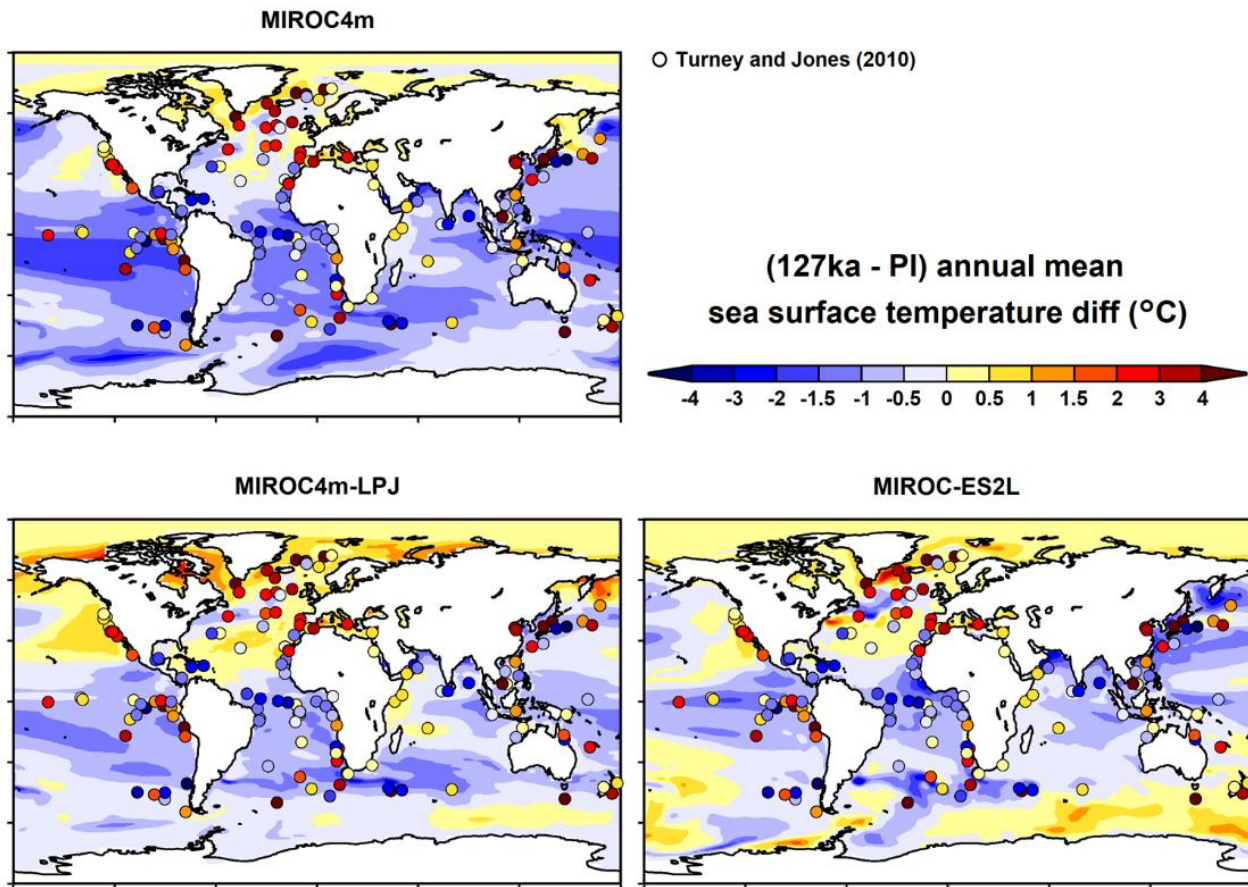
Figure 8: Annual sea surface temperature change in 127ka from PI is compared with reconstruction by Turney and Jones
455   (2010)
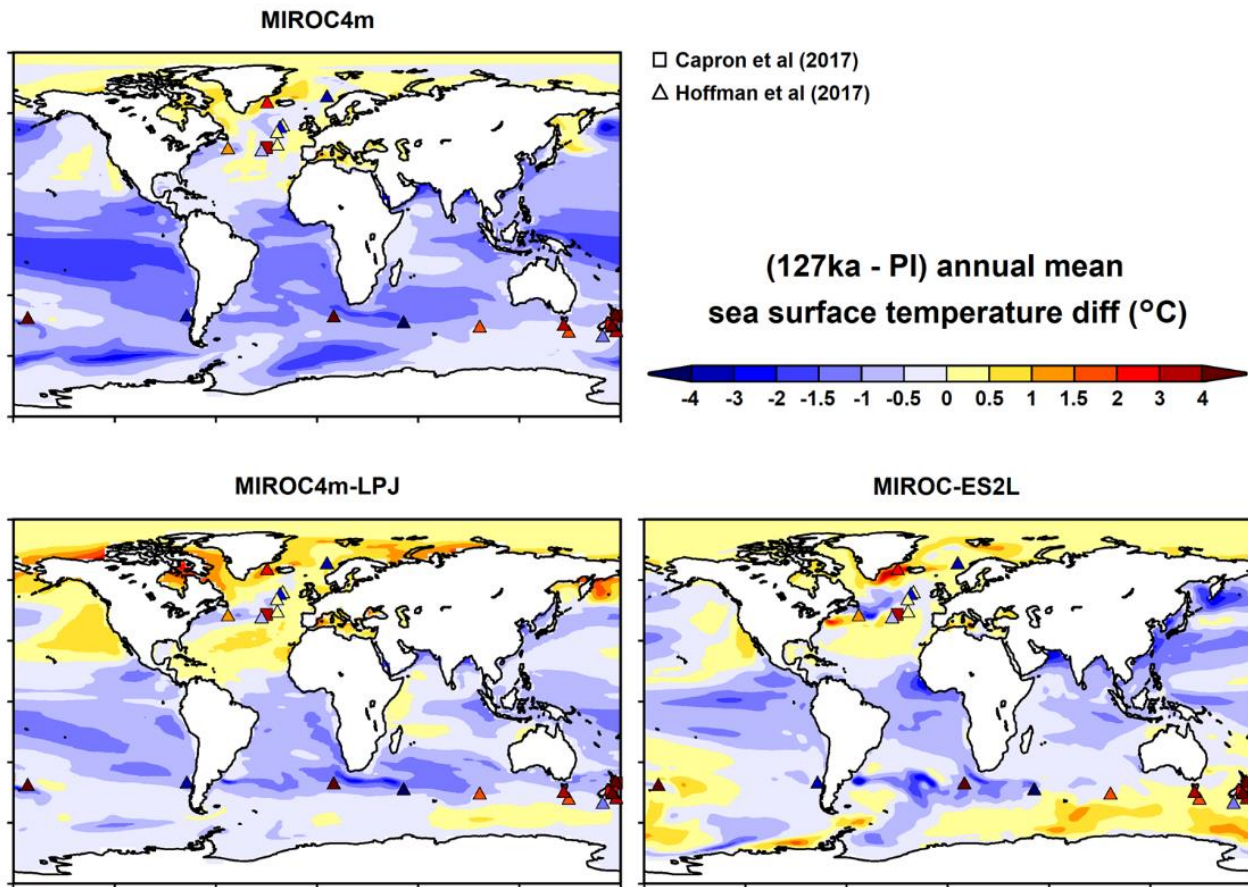
Figure 9: As same as Figure 8 but compared with reconstruction by Capron et al. (2017) and Hoffman et al. (2017).
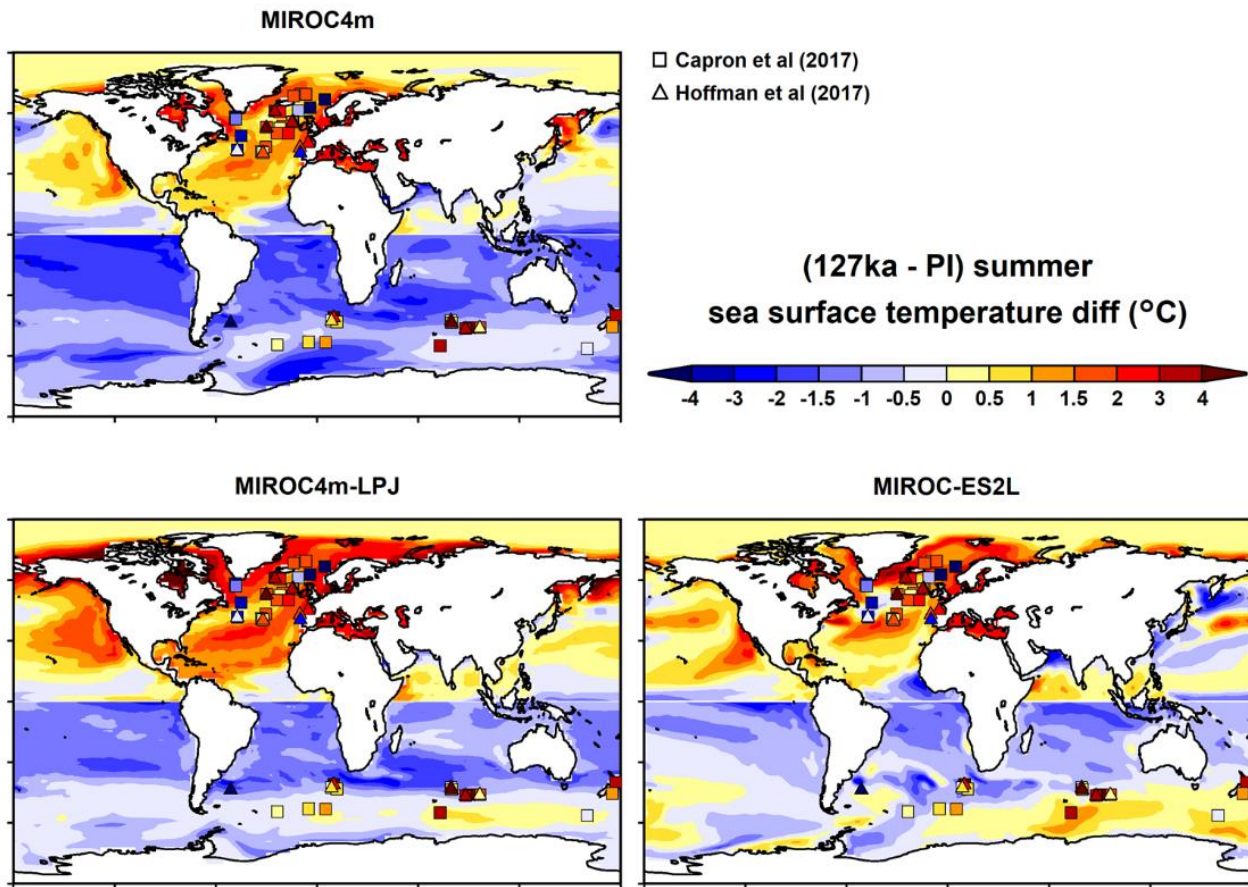
Figure 10: Summer (JJA in NH, DJF in SH) sea surface temperature change in 127k from PI is compared with reconstruction by Capron et al. (2017) and Hoffman et al. (2017).
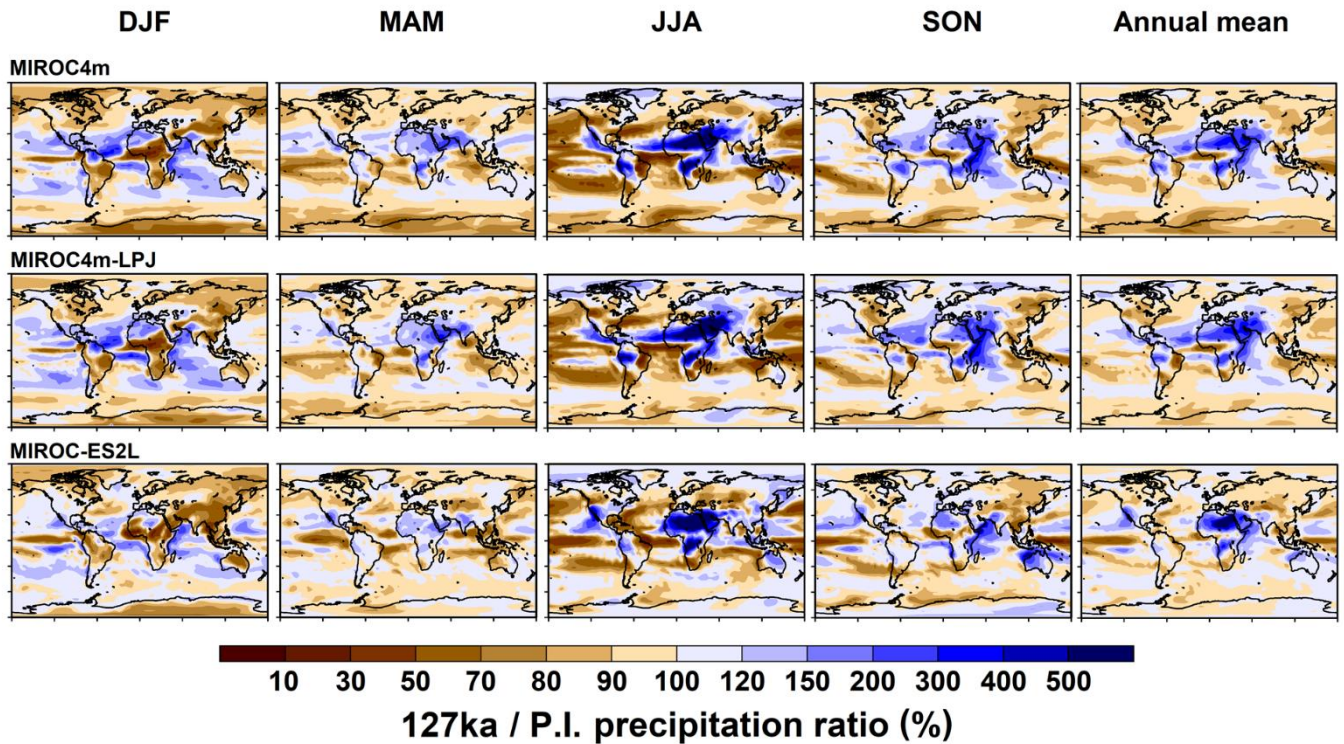
Figure 11: Annual and seasonal precipitation change is shown as the 127ka/PI ratio (%).

465
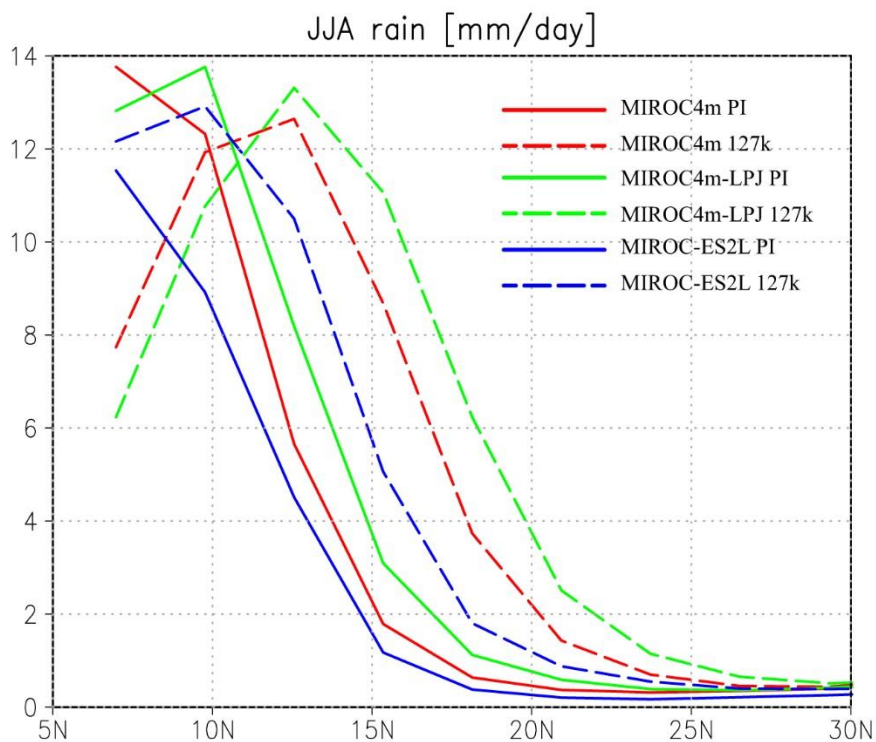
Figure 12: Zonally (30W-20E) averaged JJA precipitation (mm/day) over land at 5N to 30N.

March sea ice thickness (cm)
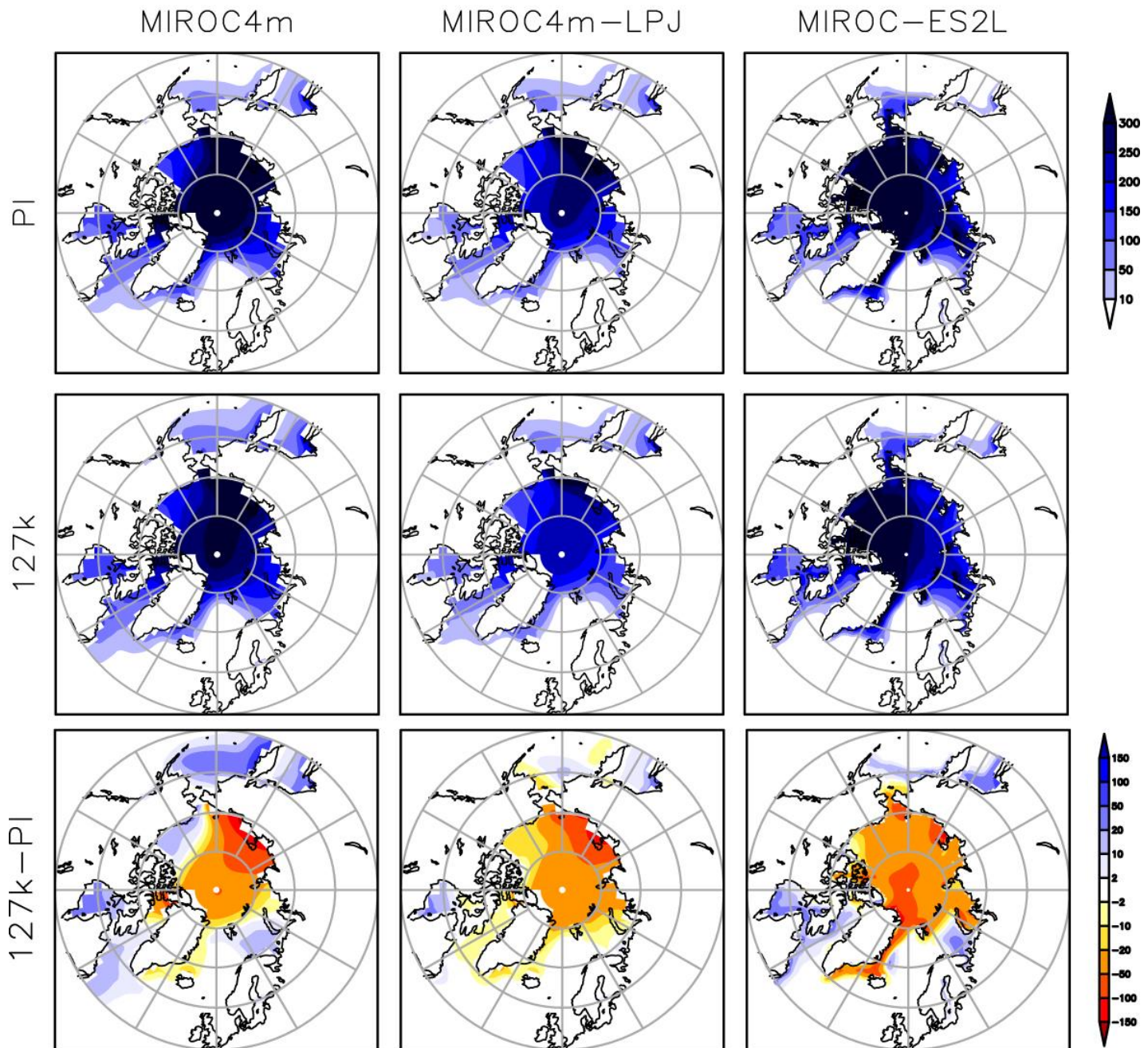
470

Figure 13: NH March sea ice thickness (cm) in PI, 127k and difference between 127k and PI are shown for three models.
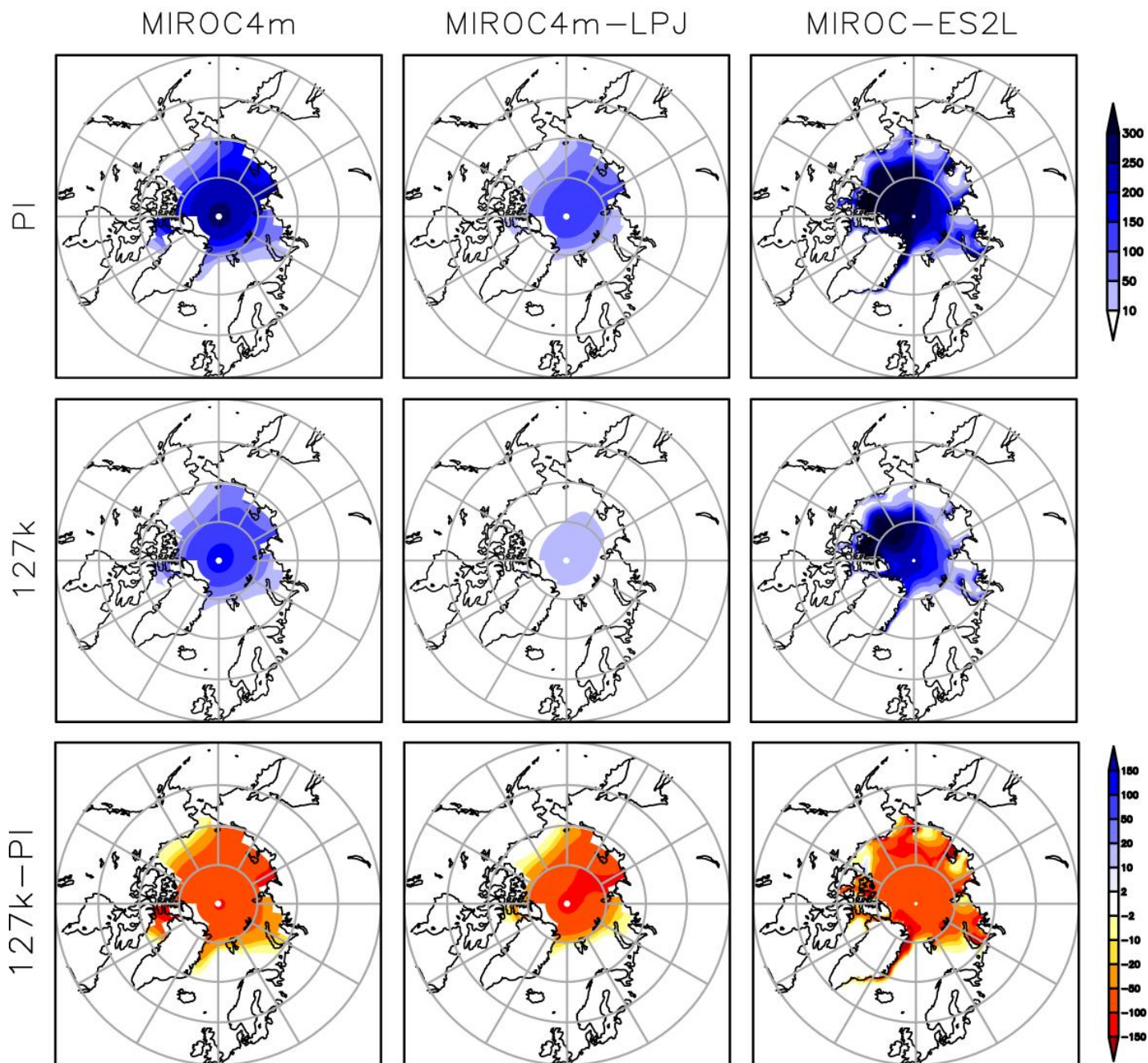
Figure 14: As same as Figure 13 but NH September sea ice thickness (cm).
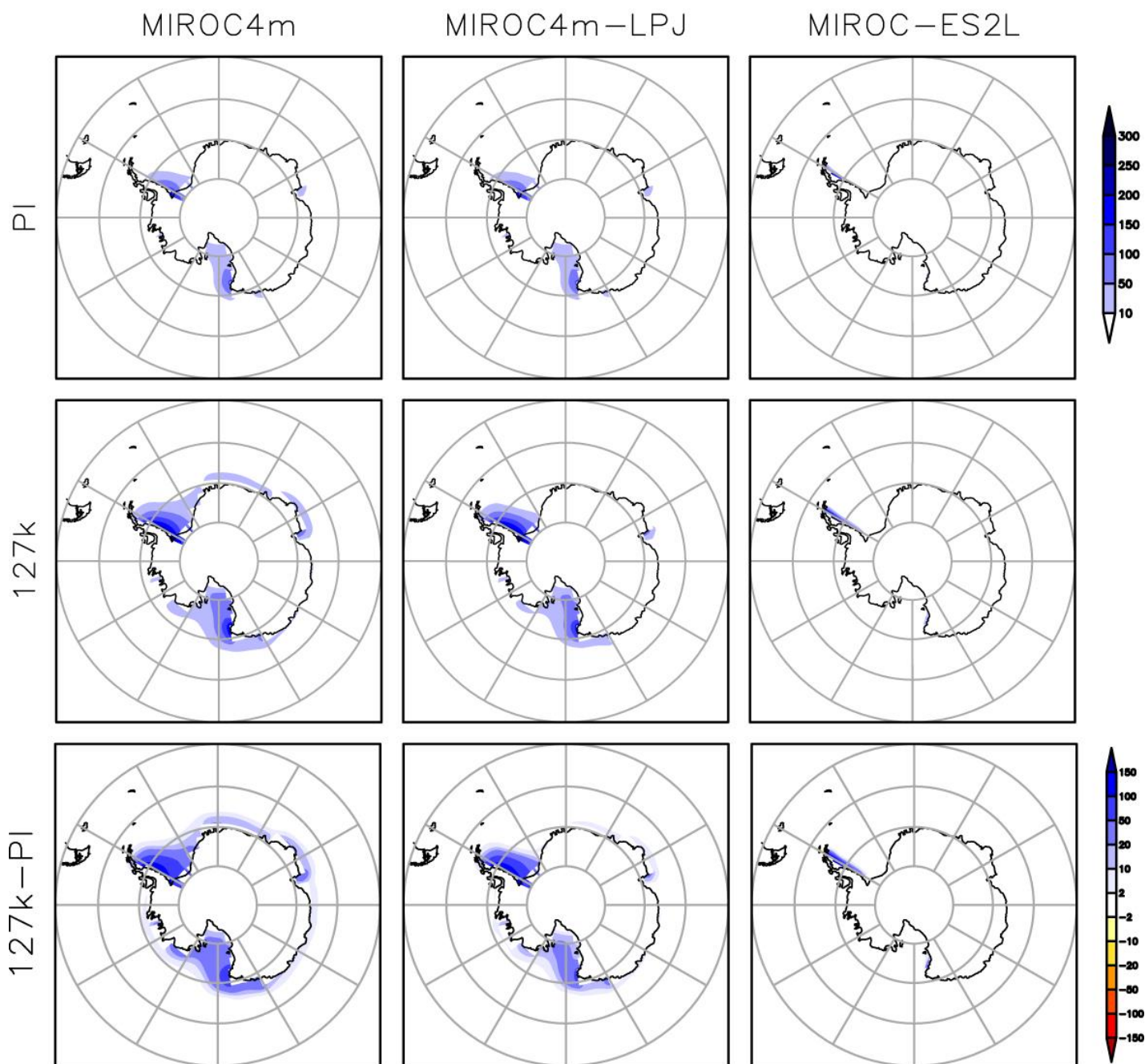
Figure 15: As same as Figure 13 but SH March sea ice thickness (cm).
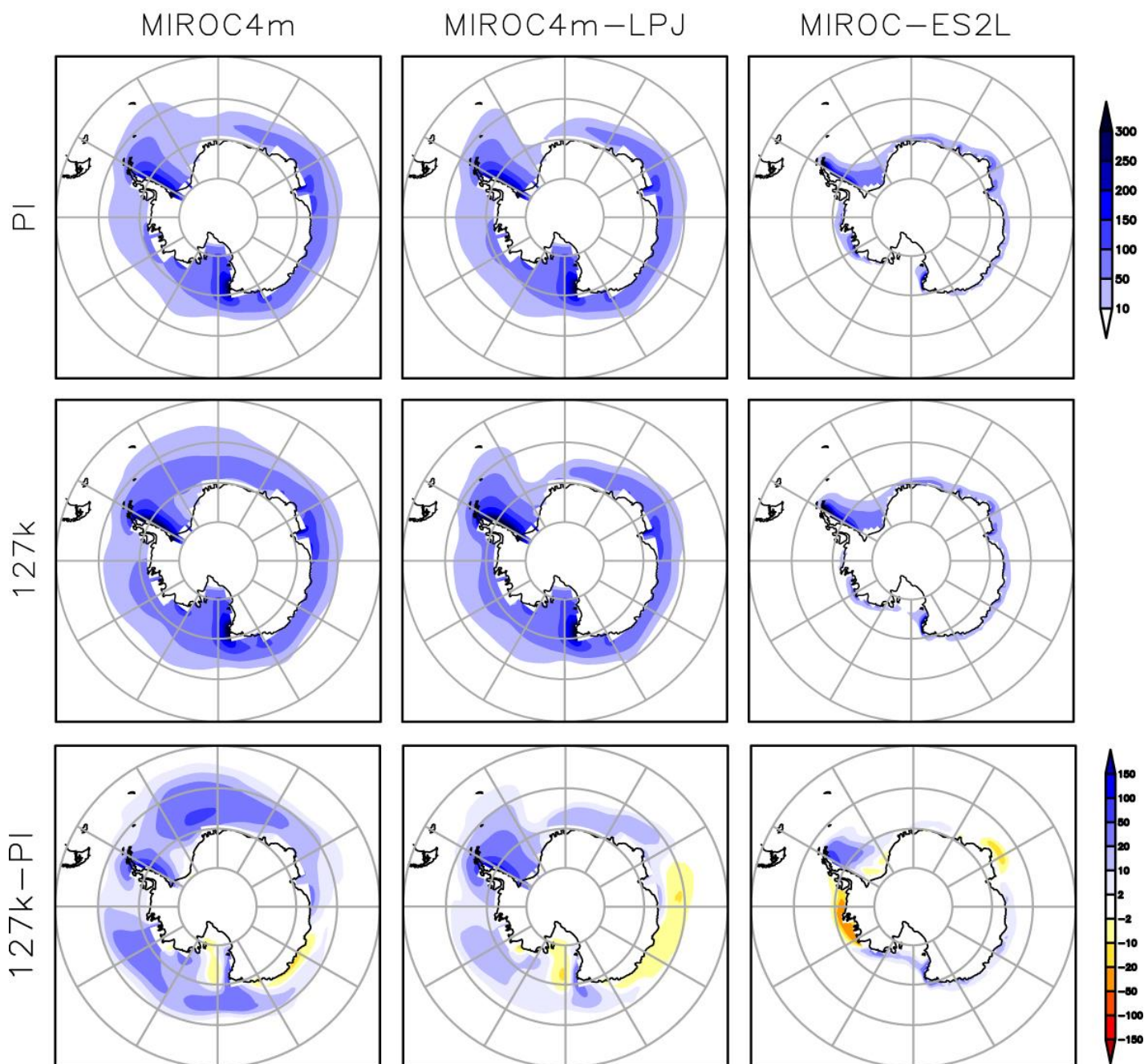
Figure 16: As same as Figure 13 but SH September sea ice thickness (cm).

485